International Journal of Infrared and Millimeter Waves (2019) 40: 306–313
https://doi.org/10.1007/s10762-019-00570-8

Monitoring the Isothermal Crystallization Kinetics of PET-A Using THz-TDS

S. Engelbrecht[1] · K.-H. Tybussek[1] · J. Sampaio[1] · J. Böhmler[1] · B. M. Fischer[1] · S. Sommer[2]

Received: 13 December 2018 / Accepted: 24 January 2019 / Published online: 30 January 2019

Abstract

Using terahertz time-domain spectroscopy (THz-TDS), we monitor the isothermal crystallization kinetics of amorphous polyethylene terephthalate (PET-A). PET-A was tempered at different temperatures and for a varied amount of time to induce a isothermal crystallization. Afterwards the THz spectra were recorded and analyzed. An adapted Avrami equation was used to analyze the spectral data to monitor the isothermal crystallization. It was found that the adapted Avrami theory is a good approach to describe the kinetics of isothermal crystallization and allows to determine kinetic parameters as with classical technologies. Therefore, we conclude that THz-TDS offers a non-destructive method to characterize the kinetics of isothermal crystallization in polymers.

Keywords Terahertz · Spectroscopy · Crystallization · Avrami equation

1 Introduction

Terahertz technology has found a wide variety of different applications in recent years. The availability of reliable sources and detectors opened the frequency range for applications in the field of telecommunication and data transfer [1–3]. Due to its non-ionizing character it also proofed useful for the bio-chemical analysis of amino-acids [4] and DNA [5]. Since many materials show characteristic fingerprints in this frequency region, the technology is very well suited for the detection and identification of dangerous substances like explosives, drugs, or counterfeit pharmaceuticals

✉ S. Engelbrecht
sebastian.engelbrecht@isl.eu

[1] French-German Research Institute of Saint-Louis ISL, F-68301 Saint-Louis, France

[2] Department of Physics and Materials Science Center, Philipps University Marburg, D-35032 Marburg, Germany

[6–8]. The technology offers a great potential for applications in the industrial sector ranging from the quality control in oils [9, 10] and paper [11] to the detection of contaminations in the food industry [12]. Plastics and in particular polymers are a material class very well suited for the characterization by THz technologies due to their dielectric properties [13]. Different aspects in the characterization and non-destructive testing of polymers by THz spectroscopy have already been presented in the literature. It was shown that the content of additives in thermoplasts [14] and elastomers [15] can be studied, the fiber orientation in compounds analyzed [16, 17] and the quality of glued or welded plastic joints controlled [18–20]. The morphology of polymers is also accesible by THz spectroscopy, allowing to draw conclusion about the crystallization [21, 22], the crystalline structure [23, 24] and phase transitions [25].

In this paper, THz time-domain spectroscopy (THz-TDS) is used to determine the kinetic parameters of the crystallization of amorphous polyethylene terephthalate (PET-A). PET, a polymer of the polyester family, exists in amorphous and semi-crystalline form. By temperature, it is possible to induce a crystallization in the amorphous PET. Furthermore, PET shows absorption features in the low THz range, originating by its molecular structure [22, 26]. These peaks are linked to the crystalline state of the polymer, so it is a suitable candidate to study the isothermal crystallization. In comparison with conventionally used techniques, like thermal analysis by differential scanning calorimetry (DSC), THz-TDS allows to obtain the kinetic parameters non-destructively. The general theory to describe the crystal growth in polymers is given by the Avrami equation [27]. The adaption of this equation to an optical Avrami equation allows to extract the critical parameters from the THz-TDS data.

2 Experimental Details

The spectroscopic measurements were carried out using a commercially available TOPTICA Teraflash system, based on a 1550-nm laser [28]. In this system, the THz radiation is generated and detected using antennas based on InGaAs photoconductive switches. A system of four off-axis parabolic mirrors was used to focus the THz beam onto the sample and the detector, respectively [29]. This systems offers a usable bandwidth of at least 4 THz with a dynamic range of 90 dB. All measurements were done under nitrogen atmosphere to prevent additional absorption caused by water vapor. The extraction of the optical parameters was done using the TERALYZER software based on a quasi-space approach introduced by M. Scheller [30]. This procedure allows the simultaneous extraction of the complex refractive index and thickness of a studied sample with high precision.

For the static analysis of the isothermal crystallization, samples of PET-A with a size of $25 \times 25\,\mathrm{mm}^2$ and a thickness of 500 µm were used. They were placed in a furnace at temperatures of 95 °C, 105 °C, 115 °C, 125 °C, 135 °C, 145 °C and 155 °C. For each temperature, 19 different samples were prepared. The tempering time varied from 0 up to 120 min. The samples were quenched in ice water directly after they were removed of the furnace to prevent any further crystallization and directly put

in the spectrometer to record the THz spectra. For the samples tempered at 125 °C, also, differential scanning calorimetry (DSC) measurements were carried out to support the findings of the THz-TDS measurments. The DSC measurements were just performed for one temperature set, since the isothermal crystallization is already well studied in the literature [31–33]. The DSC measurements were conducted using a TA Instrument DSC Q1000 with an heating rate of 10 K/min.

3 Results and Discussion

Figure 1 shows the results of the DSC measurements for the samples tempered at 125 °C for varying durations. Three distinct features can be observed. At 75 °C, the glass transition (T_g) is visible. Around 140 °C, an exothermic peak can be seen which is associated with the crystallization of the amorphous part of the sample. At this temperature, the crystall growth velocity and the probability of nucleation is well balanced, leading to the optimal conditions for a crystallization [34]. As can be seen in Fig. 1, increasing time of tempering leads to a decrease in the overall amplitude of the exothermic peak around 140 °C which corresponds to an overall higher crystallinity since less amorphous material is available for a crystallization during the heating process of the DSC. Correspondingly, also, the signature of the glass transition becomes weaker for longer tempering times. At temperatures larger than 235 °C, all studied samples start the melting process. The observed values of PET found during this study agree very well to the ones found in the literature [35].

Figure 2 shows the (a) refractive index and (b) absorption coefficient of PET at THz frequencies in its amorphous form, as well as in its semi-crystalline form. The

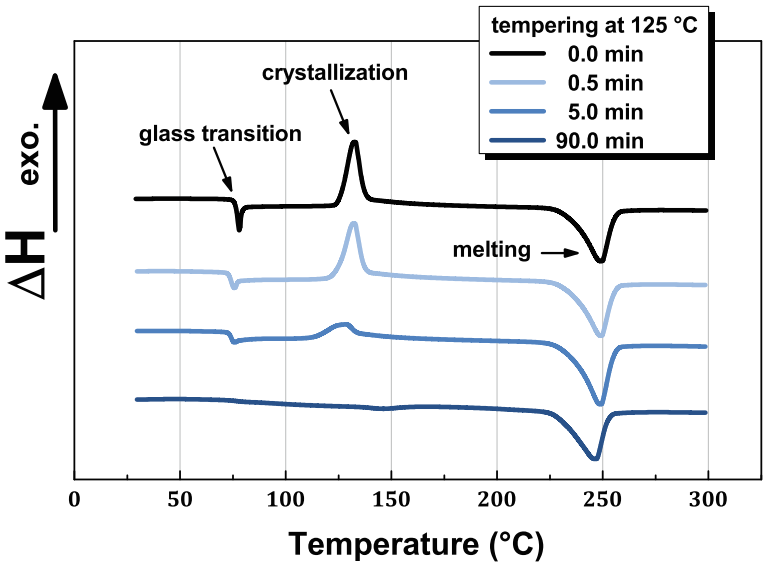

Fig. 1 DSC measurements of PET-A tempered at 125 °C after 0 min, 0.5 min, 5 min and 90 min

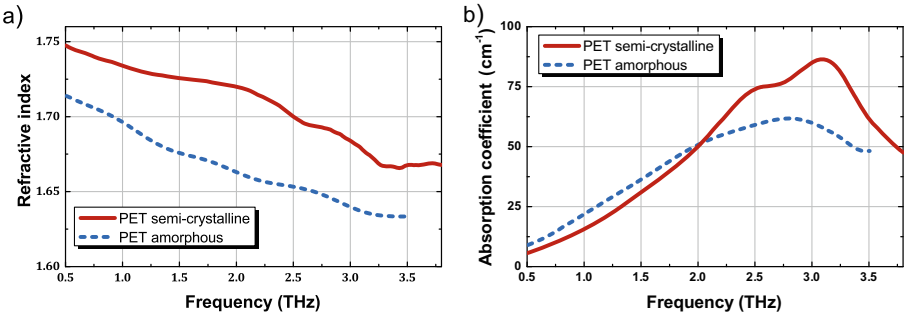

Fig. 2 Frequency dependence of **a** refractive index and **b** absorption coefficient of PET-A in semi-crystalline and amorphous form

semi-crystalline form was obtained by tempering the amorphous sample for 6 h at 150 °C. The crystallinity of the semi-crystalline sample in Fig. 2 was around 40% as determined by DSC measurements. Here, it has to be noted that the obtained value for the partial crystallinity strongly depends on the used temperature for the tempering process. For the amorphous sample, no crystallinity could be observed. As can be seen in Fig. 2, the untreated sample just has a single feature, a broad absorption peak centered around 2.7 THz. From previous studies in the far infrared, this feature could be attributed to the torsional vibration of the benzene ring in the PET molecule [36]. The tempering process induces the formation of crystalline structures in the sample, changing the THz response. Here, two absorption peaks, at 2.5 THz and 3.1 THz, can be identified. These absorption bands are already described in the literature and were first associated with phonon-like vibrational modes of the crystalline areas in the polymer [36]. Today, a model is used describing the absorption bands as coupled oscillations of single molecular groups, which propagate similar to phonons in classical solid-state physics [37].

A general theory to describe the crystal growth in polymers is given by the Avrami equation [27]:

$$\chi = \frac{m_C}{m_0} = 1 - \exp\left[-Kt^n\right], \tag{1}$$

where χ is a measure of the partial crystallinity, m_C the mass of the crystallites and m_0 the overall mass of the sample. K and n give the crystallization rate and Avrami coefficient, respectively. While K is just accessible by experiments, n can be linked by theoretical considerations to the geometrical shape of the built crystallites [38]. Equation 1 is derived by the assumption of a homogeneous distribution of the crystal nuclei and a constant density and shape of the crystallites. Moreover, neither a heterogeneous distribution in the beginning of the crystallization process nor non-crystallizable parts in the melt (like additives or contaminations) are considered. Despite the rather strict constraints in the derivation of Eq. 1, the theory nevertheless turned out to be a useful tool for the experimental characterisation of crystallization processes in polymers [38–41]. In thermal analysis, like DSC, Eq. 1 can be used to determine the partial crystallinity by integrating the area of the endothermic

crystallisation peak A_t and referencing it to the maximal value for a perfect crystallization A_∞:

$$\chi = \frac{A_t}{A_\infty}. \tag{2}$$

However, due to the absence of 100% crystalline samples, often, a theoretically determined value for A_∞ is used [42].

As it was shown in Fig. 2, the absorption bands in PET are directly related to the semi-crystalline properties of the polymer and the occurring absorption bands can be used as a measure for the crystallinity of a given sample. Due to the qualitative similar behavior of THz and the DSC data, the empirical definition of an optical partial crystallinity suggests itself. Since the overall absorption is increasing with increasing frequency, the absorption band at 2.5 THz is used for further considerations. In order to see whether the THz data can be used to further analyze the crystallization process, an optical partial crystallinity is defined as

$$\chi_{\mathrm{opt}}(t) = \frac{\alpha_{2.5\mathrm{THz}}(t) - \alpha_{2.5\mathrm{THz}}(0\,\mathrm{min})}{\alpha_{2.5\mathrm{THz}}(120\,\mathrm{min}) - \alpha_{2.5\mathrm{THz}}(0\,\mathrm{min})}. \tag{3}$$

Here, $\alpha_{2.5\mathrm{THz}}(t)$ is the absolute value of the absorption coefficient at 2.5 THz in dependence of the tempering time t. As previously discussed, a crucial point in the definition of the partial crystallinity is the value of a perfect crystalline sample. Due to the absence of perfectly crystalline samples, the optical partial crystallinity is defined here as a relative value to the endpoint of the isothermal crystallization. Following the consent in the literature, the final point of the crystallization is reached after maximal 120 min [31, 32, 38, 40]. This definition therefore does not allow to obtain absolute values for the partial crystallinity; however, it gives access to the kinetic parameters of

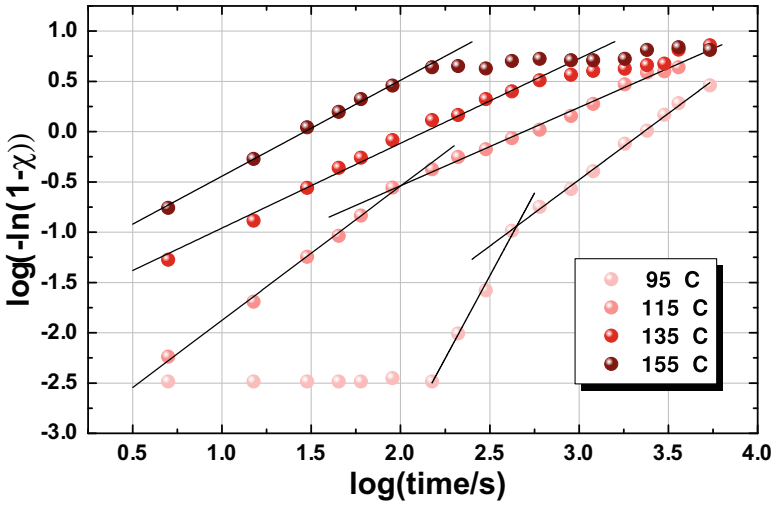

Fig. 3 Avrami plots of PET for four different temperatures

Table 1 Kinetic parameters of the optical Avrami equation extracted by linear regression

T_c (°C)	n_{opt}	K_{opt} (1/s)	$t_{1/2}^{opt}$ (s)
95	3.3	2.2E−10	771
105	1.3	6.0E−4	273
115	1.2	4.5E−4	132
125	0.9	14.1E−4	79
135	0.9	21.5E−4	45
145	0.9	32.3E−4	28
155	0.9	42.1E−4	20

the crystallization process. The combination of Eq. 1 with Eq. 3 allows the definition of an "optical" Avrami equation. After linearizing Eq. 1, this yields

$$\log\left[-\ln\left[1-\chi_{opt}(t)\right]\right] = \log\left[K_{opt}\right] + n_{opt}\cdot\log\left[t\right]. \tag{4}$$

Following Eq. 4, a double-logarithmic plot of the optical crystallinity (3) will directly yield the optical crystallization rate K_{opt}, as well as the optical Avrami coefficient n_{opt}. Figure 3 shows the Avrami plots for the PET foils tempered at different temperatures ranging from 95 up to 155 °C. Solid lines in Fig. 3 show linear regression fits for the different temperatures. Both start and end points of the linear regression (and therefore the crystallization) were defined by changes of below 5% in adjacent data points. As can be seen here, the experimental observed behavior indeed can be nicely described by Eq. 4. Moreover, it was found that for temperatures below 120 °C, the crystallization occurs in a two-step process. All these findings agree very well with already published data based on thermal analysis [38, 40]. Equation 4 allows also to define the half-life $t_{1/2}^{opt}$ after which the crystallization process is finished for 50%. Table 1 summarizes the obtained values for K_{opt}, n_{opt} and $t_{1/2}^{opt}$. The crystallization rate K_{opt} and the lifetime $t_{1/2}^{opt}$ are additionally shown in Fig. 4. It can be seen that the lifetime decreases for higher temperatures, while the crystallization rate increases, as can be expected. Since the Avrami parameters are determined by changes in the optical parameters, they cannot easily be compared with the ones obtained by thermal methods. Nevertheless, the obtained values for the

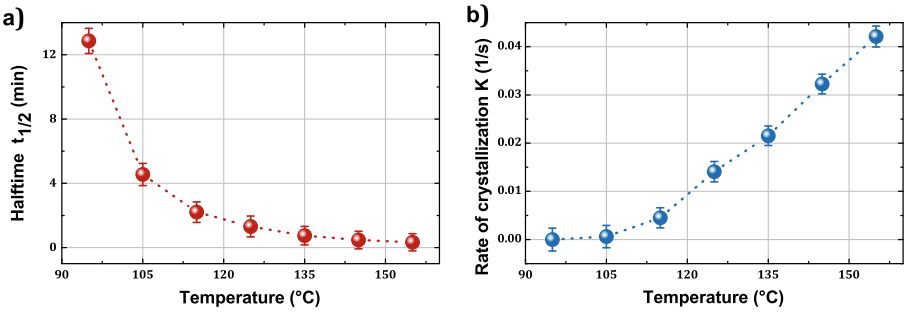

Fig. 4 Specific parameters of the crystallization kinetics extracted from the THz-TDS data of PET-A. **a** Life-time and **b** crystallization rate at different temperatures

Avrami coefficients show the same qualitative behavior and are of the same order of magnitude as the ones obtained by DSC measurements [38, 40]. The direct correlation between the optically and thermally determined Avrami parameters is still under investigation.

4 Conclusion

Terahertz time-domain spectroscopy was used to monitor the iso-thermal crystallization in amorphous polyethylene terephthalate. An optical Avrami equation was used to describe the experimental findings. The analysis of the experimental data allowed to obtain the kinetic parameters, like crystallization rate, life time and Avrami coefficient. A good agreement between the THz-TDS values and previously published values from thermal analysis was found. It can be concluded that THz-TDS is a useful tool for the non-destructive analysis of crystallization processes in polymers.

References

1. T. Kleine-Ostmann and T. Nagatsuma, J. Infrared, Millimeter, Terahertz Waves **32** (2011), 143.
2. H. Song and T. Nagatsuma, IEEE Trans. Terahertz Sci. Technol. **1** (2011), 256.
3. J. Federici and L. Moeller, J. Appl. Phys. **107** (2010), 111101.
4. K. Yamamoto, K. Timinaga, H. Sasakawa, A. Tamura, H. Murakami, H. Ohtake, and N. Sarukura, Biophys. J. Biophys. Lett. **89** (2005), L22.
5. B.M. Fischer, M. Walther, and P.U. Jepsed, Phys. Med. Biol. **47** (2002), 3807.
6. A.D. Burnett, W. Fan, P.C. Upadhya, J.E. Cunningham, M.D. Hargreaves, T. Munshi, H.G.M. Edwards, E.H. Linfield, and G. Davies, Analyst **134** (2009), 1658.
7. A.G. Davies, A.D. Burnett, W. Fan, E.H. Linfield, and J.E. Cunningham, Mater. Today **11** (2008), 18.
8. Y.C. Shen, T. Lo, P.F. Taday, B.E. Cole, W.R. Tribe, and M.C. Kemp, Appl. Phys. Lett. **86** (2005), 241116.
9. L. Tian, Q. Zhou, B. Jin, K. Zhao, S. Zhao, Y. Shi, and C. Zhang, Sci. China, Ser. G Physics, Mech. Astron. **52** (2009), 1938.
10. A. Adbul-Munaim, M. Reuter, M. Koch, and D.G. Watson, J. Infrared, Millimeter, Terahertz Waves **36** (2015), 687.
11. D. Banerjee, W. von Spiegel, M.D. Thomson, S. Schabel, and H.G. Roskos, Opt. Express **16** (2008), 9060.
12. B. S.-Y. Ung, B.M. Fischer, B. W.-H. Ng, and D. Abbott, Proc. SPIE, BioMEMS and Nanotechnology III **6799** (2007), 67991E.
13. Y.-S. Lee, *Principles of Terahertz Science and Technology*, Springer Science+Business Media, New York, 2009.
14. S. Wietzke, C. Jansen, F. Rutz, D.M. Mittleman, and M. Koch, Polym. Test **26** (2007a), 614.
15. O. Peters, M. Schwerdtfeger, S. Wietzke, S. Sostmann, R. Scheunemann, R. Wilk, R. Holzwarth, M. Koch, and B.M. Fischer, Polym. Test **32** (2013), 932.
16. C. Joerdens, M. Scheller, M. Wichmann, M. Mikulics, K. Wiesauer, and M. Koch, Appl. Opt. **48** (2009), 2037.
17. S. Katzletz, M. Pfleger, H. Phueringer, M. Mikulics, N. Vieweg, O. Peters, B. Scherger, M. Scheller, M. Koch, and K. Wiesauer, Opt. Express **20** (2012), 23025.
18. C. Jansen, S. Wietzke, H. Wang, M. Koch, and G. Zhao, Poylm. Test **30** (2011), 150.
19. D. Zhao, J. Ren, X. Qao, and L. Li, Appl. Opt. Photonics China **9674** (2015), 96741P.

20. S. Wietzke, C. Joerdens, N. Krumbholz, B. Baudrit, M. Bastian, and M. Koch, J. Eur. Opt. Soc. Publ. **2** (2007b), 2.
21. S. Sommer, T. Raidt, B.M. Fischer, F. Katzenberg, J.C. Tiller, and M. Koch, J. Infrared, Millimeter, Terahertz Waves **37** (2015), 189.
22. S. Wietzke, M. Reuter, N. Nestle, E. Klimov, U. Zadok, B.M. Fischer, and M. Koch, J. Infrared, Millimeter, Terahertz Waves **32** (2011a), 952.
23. S. Wietzke, C. Jansen, M. Reuter, T. Jung, D. Kraft, S. Chatterjee, B.M. Fischer, and M. Koch, J. Mol. Struct. **1006** (2011b), 41.
24. H. Hoshina, S. Ishii, S. Yamamoto, Y. Morisawa, H. Satu, T. Uchiyama, Y. Ozaki, and C. Otani, IEEE Trans. Terahertz Sci. Technol. **3** (2013), 248.
25. S. Wietzke, C. Jansen, T. Jung, M. Reuter, B. Baudrit, M. Bastian, S. Chatterjee, and M. Koch, Opt. Express **17** (2009), 19006.
26. V. Hoffmann, W. Frank, and W. Zeil, Kolloid-Zeitschrift **241** (1970), 1044.
27. M. Avrami, J. Chem. Phys. **7** (1939), 1103.
28. N. Vieweg, F. Rettich, A. Deninger, H. Roehle, R. Dietz, T. Goebel, and M. Schell, J. Infrared, Millimeter, Terahertz Waves **35** (2014), 823.
29. P.U. Jepsen, D.G. Cooke, and M. Koch, Laser Photonics Rev. **5** (2011), 124.
30. M. Scheller, Journal of Infrared, Millimeter and Terahertz Waves **35** (2014), 638.
31. S.A. Jabarin, J. Appl. Polym. Sci. **34** (1987), 85.
32. S.A. Jabarin, J. Appl. Polym. Sci. **34** (1987), 97.
33. N.W. Hayes, G. Beamson, D.T. Clark, D.S.-L. Law, and R. Raval, Surf. Interfac Anal. **24** (1996), 723.
34. Y. Long, R.A. Shanks, and Z.H. Stachurski, Prog. Polym. Sci. **20** (1995), 651.
35. G.W. Ehrenstein, G. Riedel, and P. Trawiel, *Thermal analysis of plastics*, Carl Hanser Verlag, Munich, 2004.
36. W. Frank and D. Knaupp, Berichte der Bunsengesellschaft für Phys. Chemie **79** (1975), 1041.
37. W.F. Frank, W. Strohmeier, and M. Hallensleben, Polymer (Guildf.) **22** (1981), 615.
38. R.M.R. Wellen and M.S. Rabello, J. Mater. Sci. **40** (2005), 6099.
39. M. Rabello and J. White, Polymer (Guildf). **42** (1997), 9423.
40. X. Lu and J. Hay, Polymer (Guildf). **42** (2001), 9423.
41. S. Liu, Y. Yu, Y. Cui, H. Zhang, and Z. Mo, J. Appl. Polym. Sci. **70** (1998), 2731.
42. B. Wunderlich, *Thermal analysis of polymeric materials*, Springer, Berlin, 2005.